Effect of uniform distributions of bonded and debonded fibers on the growth of the fiber/matrix interface crack in thin UD laminates with different fiber contents under transverse loading

Luca Di Stasio[a,b], Janis Varna[b], Zoubir Ayadi[a]

[a]*Université de Lorraine, EEIGM, IJL, 6 Rue Bastien Lepage, F-54010 Nancy, France*
[b]*Luleå University of Technology, University Campus, SE-97187 Luleå, Sweden*

Abstract

Priority: 1

Target journal(s): Composites Part B: Engineering, Composites Part A: Applied Science and Manufacturing, Composite Structures, Journal of Composite Materials, Composite Communications

Keywords: Polymer-matrix Composites (PMCs), Thin-ply, Transverse Failure, Debonding, Finite Element Analysis (FEA)

1. Introduction

Stimulated by the ever more stringent requirements in terms of weight and mechanical performances of the aerospace industry, the composite community has turned its attention in recent years to *thin ply* laminates and alternative design approaches are now considered based on this non-conventional laminate in applications ranging from cryogenic pressure vessels [1], to airplanes' wings [2], and even reusable space launchers [3].

Thin ply laminates are the result of a technological innovation, the *spread tow technology*, which consists in opening or spreading the tows in which fibers (carbon, glass, aramid, basalt among others) are usually shipped in into very thin tapes then used for laminate production. Ply thicknesses of less than 50 μm

can be mass-produced, and record thicknesses of around $20 - 25$ μm, or $\sim 4 - 5$ times the average fiber's diameter, have been achieved. The technique in its current form, sometimes referred to as "FUKUI method" from the name of the

₁₅ Japanese prefecture it originated in, was firstly proposed towards the end of 1990s [4] and perfected in subsequent decade [5, 6].

2. RVE models & FE discretization

### 2.1. Introduction & Nomenclature

₂₀ In this paper, we analyze debond development in unidirectional (UD) composites subjected to in-plane transverse tensile loading. The interaction between debonds in UD composites is studied developing models of different Repeating Unit Cells (RUC) of laminates where only the central fiber in the cell has a damage in the form of a fiber/matrix interface crack (debond). The compos-

₂₅ ite RUC may be repeating in the transverse direction only (representing an ultra-thin composite) or repeating also in the composite thickness direction, representing an infinite composite in a limiting case. Thus, the conditions at the UD composite's upper and lower boundaries are one of the parameters for the investigation. The used RUCs allow for the consideration of the composite

₃₀ with debonds as a sequence of damaged and undamaged rows, each row with only one fiber in the thickness direction. Since all of these RUCs feature regular microstructures with fibers placed according to a square-packing tiling, they are Representative Volume Elements (RVE) of composites with a certain distribution of debonds. Introducing in-plane coordinates x and y, where x is in

₃₅ the transverse direction of the UD composite under consideration, the strain in the y-direction due to a load in the x-direction is small, due to the very small minor Poissons ratio of the UD composite. Additionally, debonds are considered to be significantly longer in the fiber direction than in the arc direction. Therefore, we use 2D models under the assumption of plane strain, defined in

₄₀ the $x - z$ section of the composite. Thus, the analysis presented applies to long

2

debonds, with a focus on understanding the mechanisms of growth along its arc direction. The composites are subjected to transverse tensile strain, applied as a constant displacement in the x-direction along the vertical boundary of the RUC as shown in Figure 1 to 4. As the models are differentiated by the number of layers of fibers and by the spacing between debonds along the vertical and horizontal directions, the corresponding RUCs can be distinguished from each other based on the number n of fibers in the horizontal direction and k in the vertical direction. Furthermore, the horizontal surfaces can be either free or vertical displacement coupling can be applied. We thus introduce the common notation $n \times k - free$ and $n \times k - coupling$ to denote a RUC with $n \times k$ fibers and, respectively, a free upper surface or kinematic coupling applied to it. The specific combinations of particular choices of n, k, and boundary conditions are detailed in Section 2.2, together with the corresponding models of damaged composite they are representing.

2.2. Models of Representative Volume Element (RVE)

The first two models feature, as shown in Fig. 1, an ultra-thin UD laminate with only one row of fibers across its thickness, $k = 1$. This is quite an extreme model from the microstructural point of view; however, it allows to focus the analysis on the interaction between debonded fibers placed along the x-direction. Furthermore, as the horizontal surfaces are considered free, the interaction is stronger in this case than in any other, making the predictions of this model rather conservative. In retrospective, if only 20 years ago such a model would have been considered too abstracted from the physical reality, the recent advancements in the spread tow technology make this approach appealing also as a limiting case for practical considerations.

In the first sub-model, Fig. 1a, every n^{th} fiber in the composite is partially debonded on alternating sides of the fiber. The symmetries of the model allow the use of the upper part of the RUC. It is highlighted by blue lines in Fig. 1 to 3. Following the notation introduced in Section 2.1, we will refer to this model as $n \times 1 - free$. In the second sub-model $n = 1$, Fig. 1b, and a debond

3
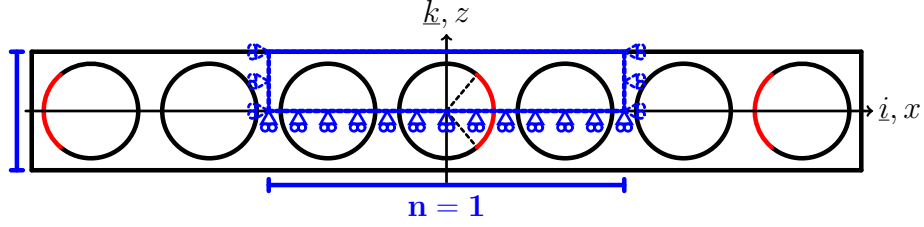
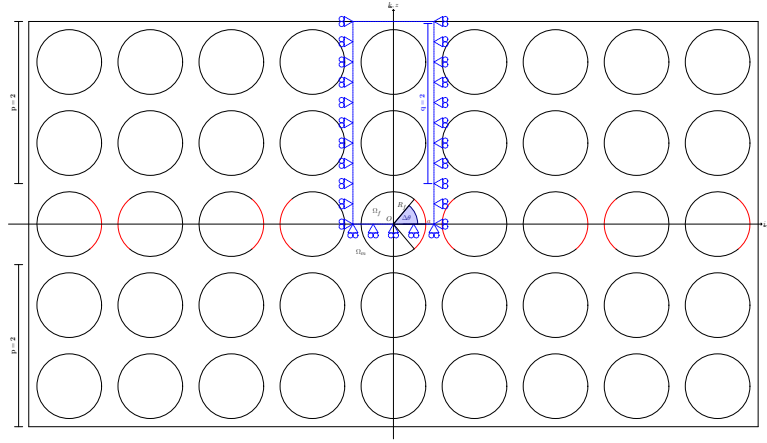(a) Single row of fibers with a debond appearing every m fibers.
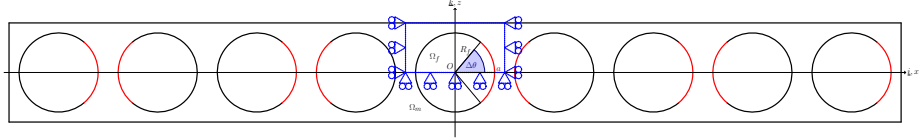
(b) Single row of fibers with debonds appearing on each fiber.

Figure 1: Models of ultra-thin UD composites with a single "row" of fibers and debonds repeating at different distances. The corresponding repeating element (RUC) is highlighted in blue, while debonds are represented in red.

appears on each fiber on alternating sides and the corresponding RUC contains only one fiber. We will refer to this model as $1 \times 1 - free$.

The second set of models in Fig. 2 and Fig. 3 considers laminates with multiple rows of fibers across the thickness: a finite number of rows in the first two sub-models in Fig. 2; an infinite number in the model of Fig. 3. In Fig. 2a, the RUC contains $n = 1$ fiber in the x-direction, k fibers across the thickness and the central fiber is debonded. This model will be referred to in the following as $1 \times k - free$. Thinking in terms of rows, in this model we have a central row where each fiber is debonded. This rows is surrounded from each side by $(k-1)/2$ rows with perfectly bonded fibers. In the sub-model in Fig. 2b, each nth fiber in the central row is debonded and this row is surrounded by $(k-1)/2$ rows of undamaged fibers from each side. We will refer to this model as $n \times k - free$ (because the horizontal boundary of the RUC is free of any constraint).

Finally, the model in Fig. 3 considers an UD composite with an infinite number of rows; all of them with partially debonded fibers. As all fibers have debonds, the corresponding RUC is made of a single partially debonded fiber

4

(a) Multiple rows of fibers with debonds appearing on each fiber beloging to the central row.
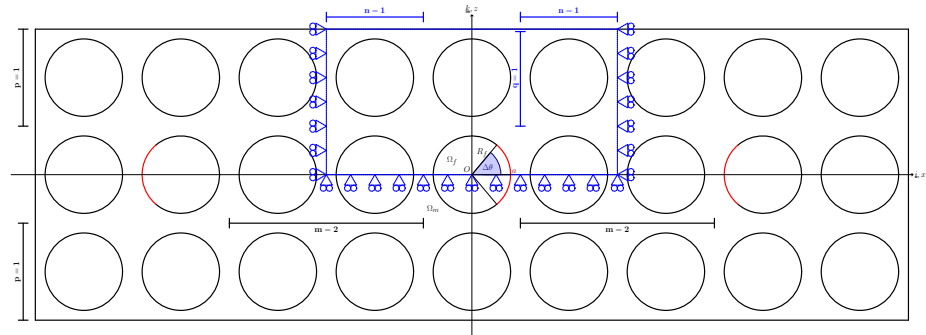
(b) Mutiple rows of fibers with a debond appearing every m fibers within the central row.

Figure 2: Models of UD composites with different "rows" of fibers and debonds repeating at different distances. The corresponding repeating element (RUC) is highlighted in blue, while debonds are represented in red.

with kinematic coupling conditions applied to the upper boundary to assure periodicity. This model is referred to as $1 \times 1 - coupling$.

2.3. Finite Element (FE) discretization

⁹⁰ Each RUC is discretized using the Finite Element Method (FEM) within the Abaqus environment, a commercial FEM package [7]. The length l and height

Figure 3: Model of UD composites with an infinite number of "rows" of fibers and debonds appearing on each fiber. The corresponding repeating element (RUC) is highlighted in blue, while debonds are represented in red.

h of the model are determined by number of fibers n in the horizontal direction and k across the thickness (see 2.2) according to Eq. 1:

$$l = 2nL \qquad h = 2kL; \tag{1}$$

where the reference length L, see Fig. 4a, is defined as a function of the fiber volume fraction V_f and the fibers' radius according to

$$L = \frac{R_f}{2}\sqrt{\frac{\pi}{V_f}}. \tag{2}$$

The fibers' radius R_f is assumed to be the same for each fiber present in the model and equal to 1 μm. The latter value is not physical and it has been chosen for simplicity. It is worth to note at this point that, in a linear elastic solution as the one presented here, the ERR is proportional to the geometrical dimensions and recalculation of the ERR for fibers of any size thus requires a simple multiplication. Furthermore, notice that the relationships in Eqs. 1 and 2 ensure that the local and global V_f are everywhere equal.

The debond is placed symmetrically with respect to the x axis (in red in 4a) and has an angular size of $\Delta\theta$ (the full debond's size is thus $2\Delta\theta$). For large debond's sizes ($\geq 60° - 80°$), a region of variable size $\Delta\Phi$ appears at the crack tip in which the crack's faces are in contact and slide on each other. Due to

6

(a) Schematic of the model with its main parameters.

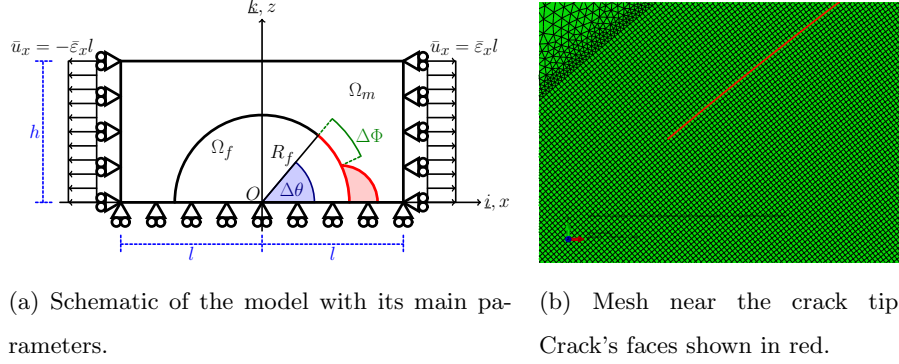(b) Mesh near the crack tip. Crack's faces shown in red.

Figure 4: Details and main parameters of the Finite Element model.

its appearance, frictionless contact is considered between the two crack's faces to allow free sliding and avoid interpenetration. Symmetry with respect to the x axis is applied on the lower boundary and kinematic coupling on the x-displacement along the left and right sides. The upper boundary is in general free, except for the model $1 \times 1 - coupling$ (Fig. 3) which requires kinematic coupling of vertical displacements also on the upper side. Constant transverse strain $\bar{\varepsilon}$ equal to 1% is applied to the right and left sides by means of an imposed x-displacement of, respectively, $\pm \bar{\varepsilon} l$.

Table 1: Summary of the mechanical properties of fiber and matrix.

Material	$E\,[GPa]$	$G\,[GPa]$	$\nu\,[-]$
Glass fiber	70.0	29.2	0.2
Epoxy	3.5	1.25	0.4

The model is meshed using second order, 2D, plane strain triangular (CPE6) and rectangular (CPE8) elements. A regular mesh of quadrilateral elements with an almost unitary aspect ratio is required at the crack tip, as shown in Fig. 4b. The angular size δ of an element in the crack tip region is always equal to 0.05°. The crack faces are modeled as element-based surfaces and a small-sliding contact pair interaction with no friction is established between them. The Mode I, Mode II and total Energy Release Rates (ERRs) (respectively referred

7

to as G_I, G_{II} and G_{TOT}) represent the main output of the FEM analysis; they are evaluated using the VCCT technique [8] implemented in a custom Python routine and, for the total ERR, the J-integral [9] by application of the Abaqus built-in functionality. A glass fiber-epoxy system is considered in every model, and it is assumed that their response lies always in the linear elastic domain. The properties used are listed in Table 1.

2.4. Validation of the model

The model is validated in Fig. 5 against the results reported in [10], obtained with the Boundary Element Method (BEM) for a single fiber with a symmetric debond placed in an infinite matrix. This situation is modeled using the *free* RVE with $V_f = 0.0079\%$, which corresponds to a RUC's length and height of ~ 100.

To allow for a comparison, the results are normalized following [10] with respect to a reference Energy Release Rate G_0 defined as

$$G_0 = \frac{1 + k_m}{8\mu_m} \sigma_0^2 \pi R_f \tag{3}$$

where μ is the shear modulus, k is the Kolosov's constant defined as $3 - 4\nu$ for plane strain conditions, R_f is the fiber radius and the index m refers to the properties of the matrix. σ_0 is the stress at the boundary, computed as the average of the stress extracted at each boundary node along the right side (arithmetic average as nodes are equispaced by design along both the left and right sides). The agreement is good: the difference between the BEM solution, which is considered more accurate, and the FEM solution does not exceed 5%. The ERRs' maxima are in the same positions and the size of the contact zone is the same. Nevertheless, an analysis of phenomena leading to less than 5% differences in ERR would not be reliable and, therefore, it is not recommended.
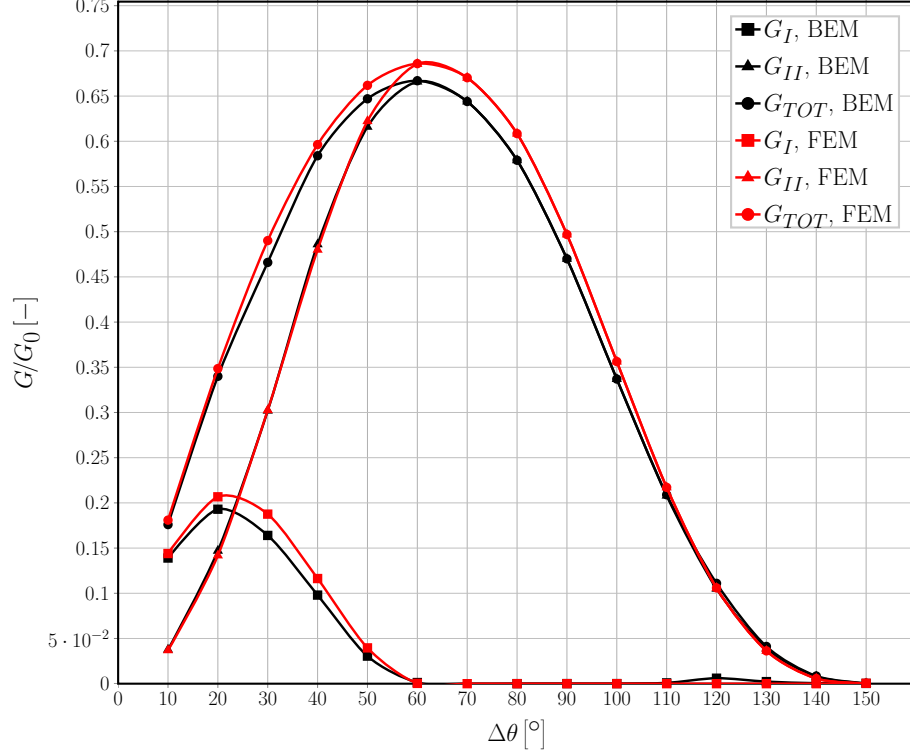
Figure 5: Validation of the single fiber model for the infinite matrix case with respect to the BEM solution in [10].

3. Results & Discussion

3.1. Effect of Fiber Volume Fraction

As shown in Figs. 6 and 7, respectively for Mode I and Mode II, the fiber content has a drastic effect on the Energy Release Rate at the tip of the fibre/matrix
150 interface crack. The effect of four levels of fiber volume fraction are compared, 30%, 50%, 60% and 65%, on two microstructural models: a $11 \times 11 - free$ (every 11th fiber in the central fiber row is partially debonded and, on the top of this row, we have 5 undamaged fiber rows), Figs. 6a and 7a, and a $21 \times 21 - free$ (every 21th fiber in the central fiber row is partially debonded and, on the top
155 of this row, we have 10 undamaged fiber rows), Figs. 6b and 7b.

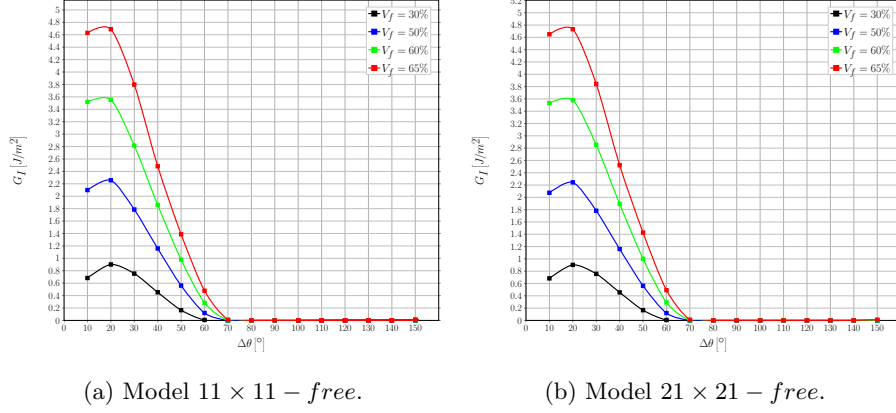Comparing Fig. 6a with 6b, and Fig. 7a with 7b, we can observe that the

9

(a) Model $11 \times 11 - free$.

(b) Model $21 \times 21 - free$.

Figure 6: A view of the effect of fiber volume fraction on Mode I ERR in two exemplificative models, subject to an applied transverse strain ε_x of 1%.

ERRs' values are very similar for RUCs with 11 × 11 and 21 × 21 fibers, though they are slightly higher for the larger RUC where the next debonded fiber and the free surface are further away from the debonded fiber. From these results we conclude that both RUCs are large enough to represent a single debonded fiber in an infinite array of bonded fibers. Obviously, there exists a specific effect of the fiber content. For Mode I, Fig. 6, the maximum value of the ERR increases by ~ 5.2 times when V_f changes from 30% to 65%. The debond's angular size for which the peak value occurs remains unchanged at 20°, but for $V_f = 60%$ and 65% the Mode I ERR at 10° and at 20° are rather similar, approximately creating a plateau. Furthermore, increasing the fiber volume fraction delays the onset of the contact zone, which corresponds in Fig. 6 to the first value of $\Delta\theta$ for which G_I is equal to zero. For $V_f = 30%$, the contact zone first appears for a debond of 60°, similarly to what happens in the single fiber in infinite matrix model (Fig. 5). For higher fiber contents, the contact zone's onset is delayed to a debond's size approximately equal to 70°.

For Mode II, Fig. 7, the maximum value of the ERR is increases by ~ 2.1 times when V_f changes from 30% to 65%. The effect is thus similar to Mode I, but with a significantly lower magnitude. Similar to Mode I, the debond's size for which the peak value of Mode II occurs remains unchanged, at 60° for Mode
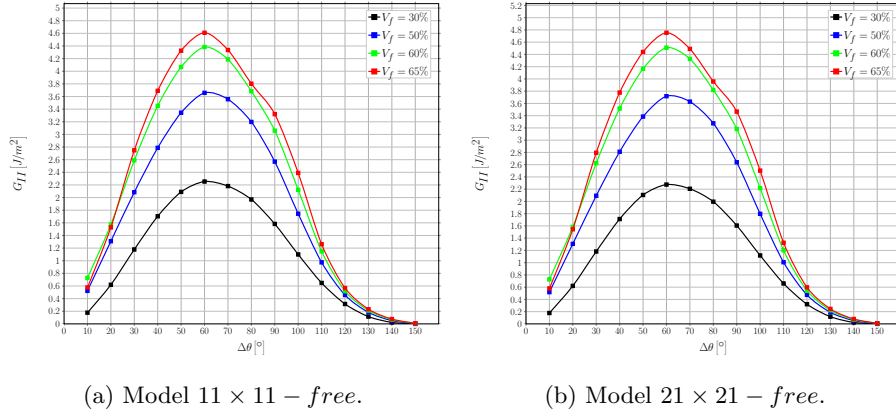
10

(a) Model $11 \times 11 - free$. (b) Model $21 \times 21 - free$.

Figure 7: A view of the effect of fiber volume fraction on Mode II ERR in two exemplificative models, subject to an applied transverse strain ε_x of 1%.

II. There is a distinct maximum in the curve and its shape does not depend on the fiber content. It is worthwhile to notice that the ratio of Mode II to Mode I peak values is $\frac{max(G_{II})}{max(G_I)} \sim \frac{2.2}{0.9} \sim 2.4$ for $V_f = 30\%$, while it is $\sim \frac{4.7}{4.7} \sim 1$ for $V_f = 65\%$. Given that the peaks occur at different debond's sizes, for which the value of the other ERR is very small or even close to zero, this means that the increase in fiber content creates a long range of very close values of the total ERR, that may have a global destabilizing effect on the debond's growth.

The general increasing trends observed in Figs. 6 and 7 are related to the fact that, given that the global and local V_f are everywhere identical in the models presented, an increase in fiber content corresponds to a decrease in the average distance between fibers. Thus, the decay of the local stress and strain fields in the matrix domain occurs over smaller lengths causing higher values at the crack tip. The difference in relative magnification between Mode I and Mode II and the delay in the contact zone's onset are instead due to the interplay between two different mechanisms, both caused by the ordered microstructural arrangement of the model. In the models considered, a fully bonded fiber is always placed along the horizontal direction, aligned with the partially debonded fiber and exactly in front of the debond. By increasing V_f, the former moves closer to the latter and for small debonds this causes a magnification of the

11

x-strain at the crack tip. For small debonds ($\leq 20° - 30°$) in fact, the crack tip is approximately normal to the x-direction and thus an increase in ε_x causes an increase in G_I. On the other hand, for large debonds ($\geq 70° - 80°$) the crack growth direction is almost aligned with the x-axis, thus a magnification in the x-strain translates into an increase of Mode II ERR. However, this increasing effect on G_{II} is partially counteracted by the presence of a fully bonded fiber on top of the debonded fiber and aligned with it. As fibers are more rigid than the sourrounding matrix, the presence of the former will restrain horizontal displacements, thus hampering strong increases in G_{II} for large debonds. Furthermore, due to the mismatch in the Poisson's ratios, the fully bonded fiber placed above generates an upward-directed component of the vertical displacement field in the matrix, which tends to open the debond and causes the delay in the contact zone's onset. The interplay between these mechanisms is governed by the average inter-fiber distance and, in turn, by the fiber volume fraction.

3.2. Interaction between debonds in UD laminates with a single layer of fibers

The interaction of debonds appearing at regular intervals in an ultra-thin UD composite with a single row of fibers is studied for Mode I (Fig. 8) and Mode II (Fig. 9) and fiber content equal to 30% (Figs. 8a and 9a) and 60% (Figs. 8b and 9b). The models treated are $3 \times 1 - free$, $5 \times 1 - free$, $7 \times 1 - free$, $11 \times 1 - free$, $21 \times 1 - free$, $101 \times 1 - free$ and $201 \times 1 - free$, corresponding respectively to a debond every 3rd, 5th, 7th, 11th, 21st, 101st and 201st fiber (Fig. 1a). Given that the upper surface of the UD row is left free, the interaction with the next RUC is stronger than in any other case and the results of this section are thus the most conservative in terms of debond's growth: the ERRs should be the largest. The effect is enhanced in composites with high V_f and especially for G_{II}: at $V_f = 60\%$ the highest G_{II} value for the $201 \times 1 - free$ composite in Fig. 9b is more than 3 times higher than the G_{II} value value for the $21 \times 21 - free$ composite in Fig. 7b. Even the maximum is shifted to larger angles. The G_I value is only 30% higher.

From both Fig. 8 and Fig. 9, it can be seen that the presence of a debond

₂₂₅ decreases the strain magnification effect discussed in Sec. 3.1 and thus reduces the value of the ERR. This phenomenon is called "crack shielding".

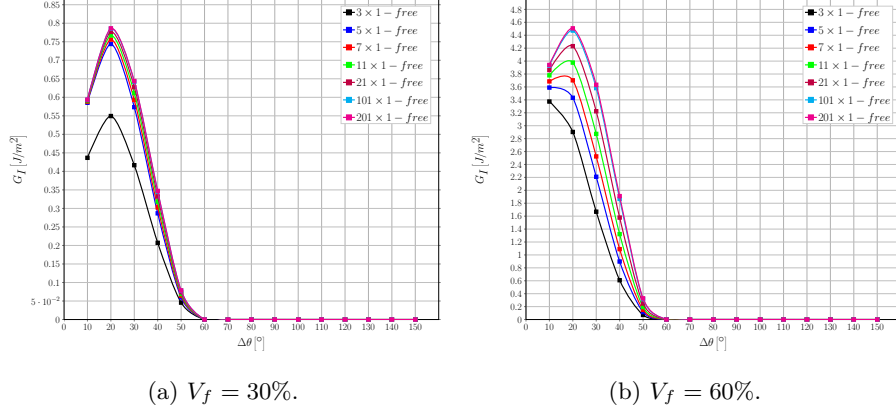(a) $V_f = 30\%$.   (b) $V_f = 60\%$.

Figure 8: Effect of the interaction between debonds appearing at regular intervals on Mode I ERR in an UD with a single layer of fibers at different levels of fiber volume fraction V_f, subject to an applied transverse strain ε_x of 1%.

For Mode I, the presence of a free surface, and inversely the absence of a fully bonded fiber along the vertical direction, implies the absence of the counteracting upward-oriented vertical component of the displacement field due ₂₃₀ to the mismatch in Poisson's ratios. This in turn translates into the constancy of the value of $\Delta\theta$ corresponding to contact zone's onset, always equal to 60°. For $V_f = 30\%$, Mode I is reduced when the spacing between debonds (in terms of fully bonded fibers in our models) decreases, but the magnitude of change is significant only when the spacing is reduced from a debond every 5th fiber to ₂₃₅ one every 3rd. For comparison, the difference of peak G_I values for $V_f = 30\%$ between $5 \times 1 - free$ and $3 \times 1 - free$ is $\sim 0.2 \frac{J}{m^2}$ (around 30% of the lower value), while between $201 \times 1 - free$ and $5 \times 1 - free$ is $\sim 0.05 \frac{J}{m^2}$ (around 7% of the lower value). A similar observation can be made for $V_f = 60\%$, but for larger spacings: no difference can be seen between the case of a debond placed ₂₄₀ every 101th and every 201th fiber. These observations suggest the existence of characteristic distance dependent on the fiber volume fraction which governs the interaction between debonds: in low V_f composites ($V_f = 30\%$) the convergence

13

to a non-interactive solution is faster (less interaction between debonded fibers in neighboring RUCs).
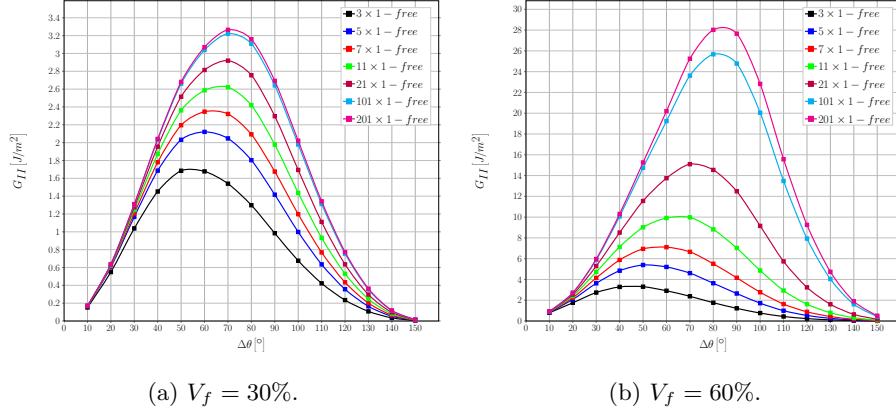

(a) $V_f = 30\%$. (b) $V_f = 60\%$.

Figure 9: Effect of the interaction between debonds appearing at regular intervals on Mode II ERR in a single-ply laminate with a single layer of fibers at different levels of fiber volume fraction V_f, subject to an applied transverse strain ε_x of 1%.

Without costraint on the upper surface, the strain magnification effect creates a larger displacement gap in the x-direction, which increases Mode II for larger debonds. When debonds are far apart, the series of rigid elements in the ultra-thin composite row (constituted by fully bonded fibers and their surrounding matrix) creates higher x-strains in the element with the debonded fiber, which in turn generates higher tangential displacements at the crack tip for larger debonds. Conversely, when debonds are closer, the strain concentration in the debonded element is more similar to the applied strain (the magnification is reduced) and the tangential displacement component at the crack tip decreases for large $\Delta\theta$. This is the mechanism behind the change in the value of $\Delta\theta$ for which the peak of G_{II} occurs: from 70° to 50° at 30%, and from 80° to 40° at 60% going from the higher to the smaller spacing of debonds. Differently from Mode I, the presence of a characteristic distance is harder to establish. For $V_f = 30\%$ (Fig. 9a), it seems reasonable to establish it at around 100 fully bonded fibers between each debond. For $V_f = 60\%$ (Fig. 9b), the difference between models $101 \times 1 - free$ and $201 \times 1 - free$ is still sizable, thus

preventing the establishment of such characteristic distance. It is possible to observe, however, that the change between $101 \times 1 - free$ and $201 \times 1 - free$ is significantly smaller than between $21 \times 1 - free$ and $101 \times 1 - free$ ($2 \left[\frac{J}{m^2} \right]$ vs $11 \left[\frac{J}{m^2} \right]$), thus suggesting the existence of the characteristic distance outside the range studied. Nevertheless, one should question wheather the single row composite with free surface is an appropriate RUC for defining the upper bound for G_{II}: G_{II} may be more affected by the free surface than by the effect of the interaction between debonds in the row.

3.3. Influence of rows of fully bonded fibers on debond's growth in RUCs with debonds in the central row

The effect of the presence of layers of fully bonded fibers on debond's growth in a line of partially debonded fibers located at mid-thickness in UD composites is studied for Mode I (Fig. 10) and Mode II (Fig. 11) and fiber content equal to 30% (Figs. 10a and 11a) and 60% (Figs. 10b and 11b). The models treated are $1 \times 3 - free$, $1 \times 5 - free$, $1 \times 7 - free$, $1 \times 11 - free$, $1 \times 21 - free$, $1 \times 101 - free$ and $1 \times 201 - free$, corresponding to a UD composite with respectively 3, 5, 7, 11, 21, 101 and 201 rows of fibers (Fig. 2a) and each fiber debonded in the central row.
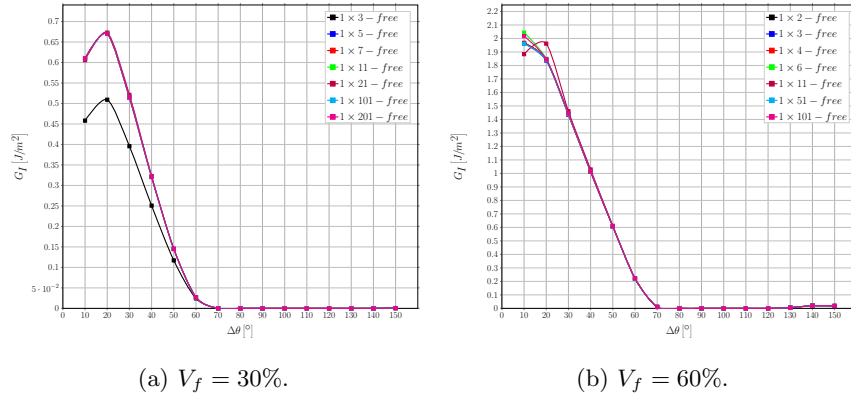

(a) $V_f = 30\%$.   (b) $V_f = 60\%$.

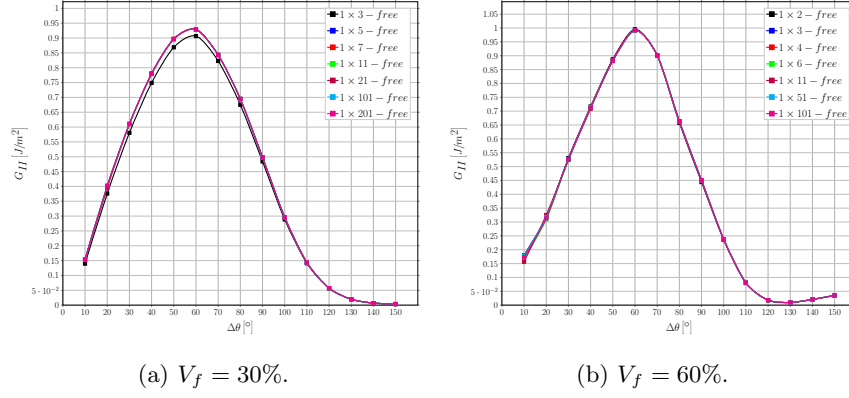Figure 10: Influence of layers of fully bonded fibers on debond's growth in Mode I ERR in a centrally located line of debonded fibers at different levels of fiber volume fraction V_f, subject to an applied transverse strain ε_x of 1%.

15

The results shown strengthen the considerations made in Sec. 3.1. It can
in fact be seen in Fig. 10 that an increasing number of bonded fibers' rows
across the thickness delays the onset of the contact zone to a debond of 70° in
size, due to the introduction of an additional positive component of the vertical
displacement which translates into an opening displacement at the debond's tip.
Comparing Fig. 9b with Fig. 11b, we observe that the presence of bonded fibers'
rows significantly reduce the G_{II} and its maximum is shifted back to 60°, thus
confirming the hypothesis in Section 3.2 that the absence of G_{II} convergence
with the increasing distance in a single-row composite is caused more by the
free surface than by the interaction between debonds.

(a) $V_f = 30\%$. (b) $V_f = 60\%$.

Figure 11: Influence of layers of fully bonded fibers on debond's growth in Mode II ERR in a
centrally located line of debonded fibers at different levels of fiber volume fraction V_f, subject
to an applied transverse strain ε_x of 1%.

The results of both Mode I and Mode II show that the introduction of
an increasing number of fully bonded fibers's rows doesn't change the ERR
calculated at the crack tip (the convergence is very fast). Some effect of the V_f
(mostly on Mode I) can be observed at low fiber content (Figs. 10a and 11a),
while for high fiber content the smaller model with only one fiber row above the
partially debonded one is already representative.

16

3.4. Interaction between debonds in UD composites with multiple rows of fibers

The interaction of debonds appearing at regular intervals in UD composites with multiple rows of fibers is investigated using different combinations of horizontal debonds' spacing and number of rows of fibers across the thickness, corresponding to the models: $3 \times 3 - free$, $5 \times 3 - free$, $5 \times 5 - free$, $7 \times 3 - free$, $7 \times 5 - free$, $7 \times 7 - free$, $11 \times 3 - free$, $11 \times 5 - free$, $11 \times 7 - free$, $11 \times 11 - free$, $21 \times 3 - free$, $21 \times 5 - free$, $21 \times 7 - free$, $21 \times 11 - free$, $21 \times 21 - free$, $101 \times 3 - free$, $101 \times 5 - free$, $101 \times 7 - free$, $101 \times 11 - free$, $201 \times 3 - free$, $201 \times 5 - free$, $201 \times 7 - free$, $201 \times 11 - free$ (Fig. 2b).

(a) G_I.   (b) G_{II}.
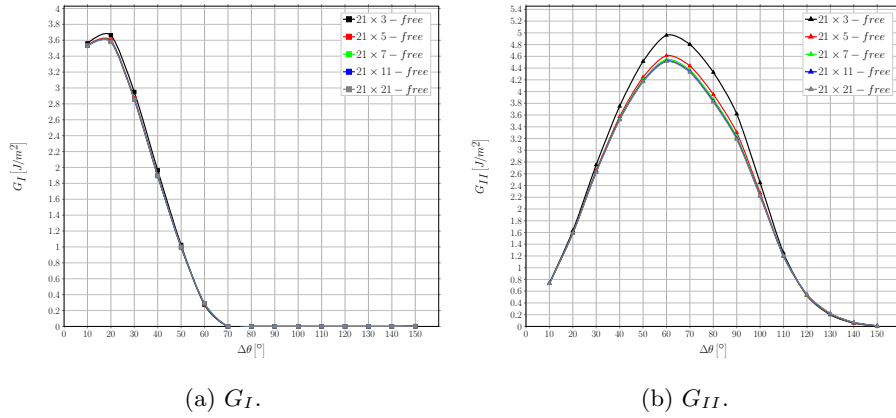
Figure 12: Effect on Mode I and Mode II ERR of the presence of an increasing number of rows of fully bonded fibers in UD composites with debonds appearing every 10th fiber (model $21 \times k - free$). $V_f = 60\%$ and $\varepsilon_x = 1\%$.

The results shown in Fig. 12 confirm the observations discussed in Sec. 3.2: the presence of fully bonded fibers across the thickness has a restraining effect on the ERR, that counteracts the magnification due to an increasing number of fully bonded fibers in the horizontal direction. The interplay is further modulated by the fiber content. For Mode I, at high fiber content the contact zone onset starts at $70°$ for $V_f = 60\%$, delayed with respect to the low fiber content case of $60°$. Comparing Fig. 12 with Fig. 10b and Fig. 11b, it is furthermore possible to observe that the number of fully bonded fibers' rows necessary to reach convergence to a non-interacting solution in the vertical direction depends on

17

the spacing of debonds in the central row. In Figures 10b and 11b the results for the $1 \times 3 - free$ model (1 row below and above) are already representative of all the other cases; in Fig. 12 the solution doesn't change anymore once at least 3 rows below and above the central one are present, when convergence in both G_I and G_{II} is required.

The results in Fig. 13 show that the converse is as well as true: the characteristic distance (in terms of fully bonded fibers) between debonds for which a non-interactive solution is attained changes in relation to the thickness of the UD composite (defined by the number of rows in the vertical direction). Mode I appears to be far less sensitive than G_{II} to the spacing of debonds in the horizontal direction when rows of fully bonded fibers are present above and below: in Fig. 13a the increase in the peak value of G_I is $\sim 8\%$ going from model $5 \times 3 - free$ to $201 \times 3 - free$, while $< 5\%$ for larger spacings. In UDs of increased thickness, Figures 13c and 13e, the variation is further reduced. For Mode II, convergence to a non-interactive solution is reached with a spacing of 100 fully bonded fibers for a UD with 3 rows of fibers across the thickness ($\frac{G_{II}^{201 \times 3}(60°) - G_{II}^{101 \times 3}(60°)}{G_{II}^{101 \times 3}(60°)} \sim 0.7\%$), of 20 fibers in a UD with 5 rows ($\frac{G_{II}^{101 \times 5}(60°) - G_{II}^{21 \times 5}(60°)}{G_{II}^{21 \times 5}(60°)} \sim 4.3\%$) and of 10 fibers in a UD with 11 rows ($\frac{G_{II}^{21 \times 11}(60°) - G_{II}^{11 \times 11}(60°)}{G_{II}^{11 \times 11}(60°)} \sim 3.4\%$).

3.5. Comparison with the single fiber model with equivalent boundary conditions

The single fiber RUC ($1 \times 1 - free$ or $1 \times 1 - coupling$) corresponds to the most damaged state of the composite, i.e. the state in which all fibers have debonds. The $1 \times 1 - free$ model represents an ultra-thin UD composite with a single row of partially debonded fibers. The $1 \times 1 - coupling$ model, where the displacement coupling is used to enforce periodic boundary conditions, represents an infinite composite.
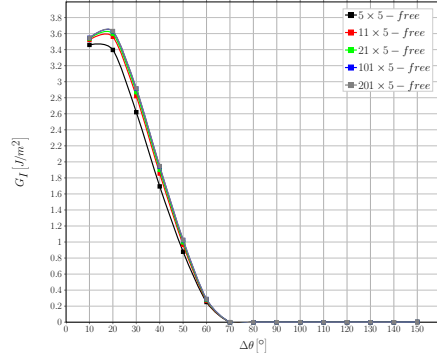
The comparison of the $1 \times 1 - free$ model with one row multi-fiber models $n \times 1 - free$ in Figure 14 show that the former provide in general the lowest value of the ERR (the highest crack shielding case) which is consistent with the trends observed in Section 3.2.
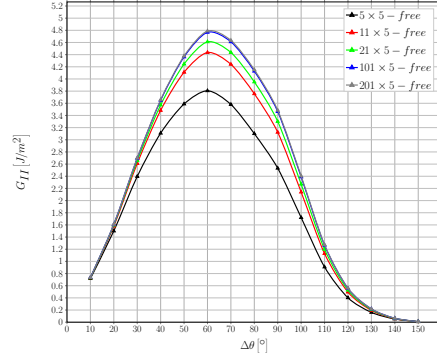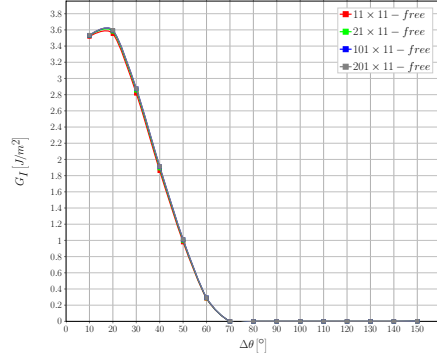
18
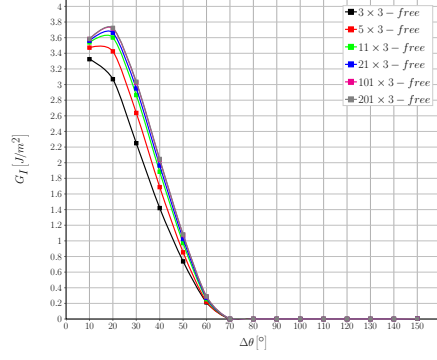
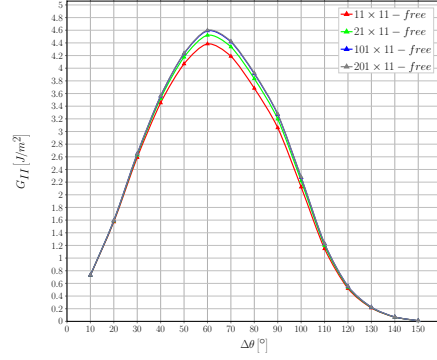(a) $k = 3$, G_I.
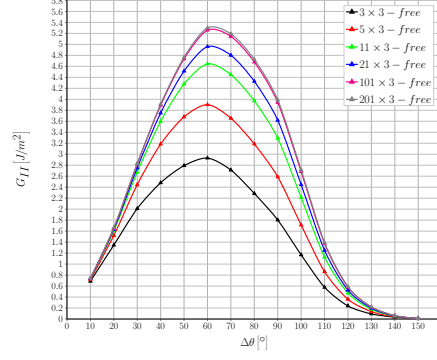
(b) $k = 3$, G_{II}.

(c) $k = 5$, G_I.

(d) $k = 5$, G_{II}.

(e) $k = 11$, G_I.

(f) $k = 11$, G_{II}.

Figure 13: Effect on Mode I and Mode II ERR of increasing the spacing between debonds appearing in the central row of fibers in a UD composite with a fixed number of rows across the thickness. $V_f = 60\%$ and $\varepsilon_x = 1\%$.
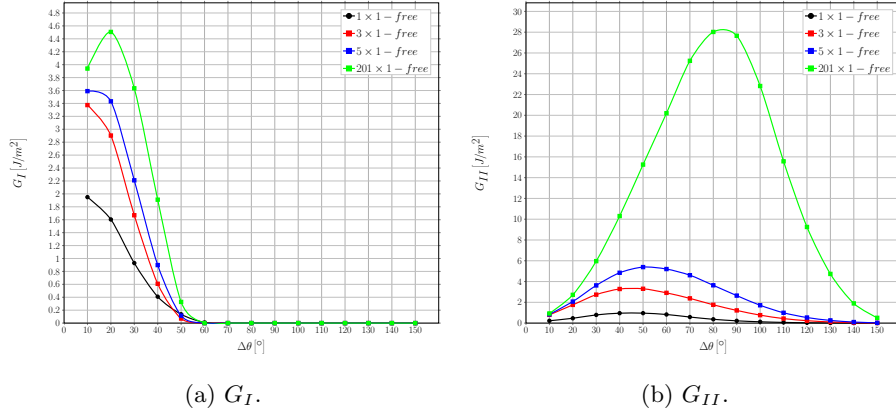
19

(a) G_I.

(b) G_{II}.

Figure 14: Comparison of the ERR between the single fiber model with free upper boundary and the multiple fibers model with fibers only on the side. $V_f = 60\%$ and $\varepsilon_x = 1\%$.

The $1 \times 1 - coupling$ model is compared with $1 \times 3 - free$ and $1 \times 201 - free$ models in Fig. 15. In all three models the distance between debonds in the x-direction is the same and the difference is in the vertical direction. The $1 \times 1 - coupling$ model describes the interaction between debonds in different rows of debonded fibers whereas the $1 \times k - free$ models describe the effect of the proximity of the composite's free surface. The Mode I ERR in the $1 \times 3 - free$ model and in the $1 \times 1 - coupling$ model is very similar, which leads to a rather surprising conclusion. In both models we have, on the top of the central one, a large amount of fibers (bonded in one case and debonded in the other case). It appears that the effect of bonded and debonded fibers on the central debond is the same. This implies that the interaction between debonded fibers in elements placed on top of each other is small. The volume fraction effect is much smaller in high fiber content composites of this type.

The same comparison for Mode II shows a sizeable difference in the range $50° - 90°$, while the results almost coincide for smaller values of $\Delta\theta$. These observations point to the evidence that debond interaction is more significant in the loading direction than in the transverse one. The lower values of G_{II} of the $1 \times 1 - coupling$ model in the range $50° - 90°$ are due to the shielding effect of a debond of the same size in the fiber just above the central one (modeled

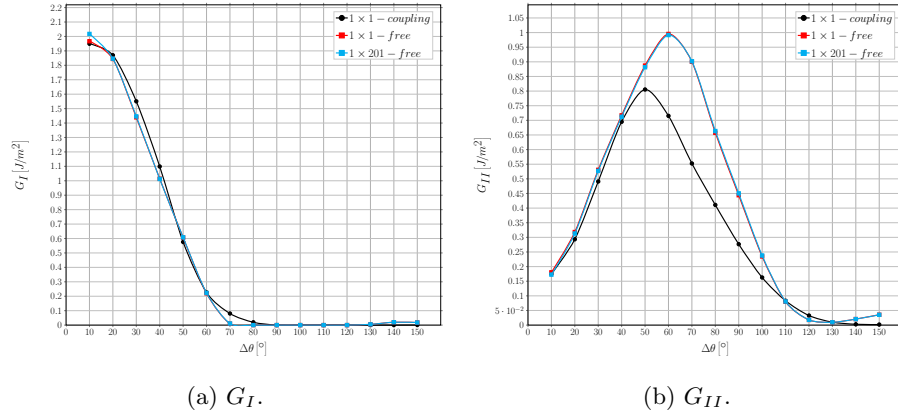20

(a) G_I.

(b) G_{II}.

Figure 15: Comparison of the ERR between the single fiber model with coupling conditions along the upper boundary and the multiple fibers model with fibers above. $V_f = 60\%$ and $\varepsilon_x = 1\%$.

by the coupling boundary condition), which leaves the strip of matrix between the two fibers free to deform away from both of them due to the Poissons effect and thus favors Mode I and reduces Mode II. This translates into the lower estimates in Fig. 15b and into the delay in the appearance of the contact zone, particularly evident in Fig. 15a.

4. Conclusions & Outlook

Acknowledgements

References

[1] D. A. McCarville, J. C. Guzman, A. K. Dillon, J. R. Jackson, J. O. Birkland, 3.5 Design, Manufacture and Test of Cryotank Components, Elsevier, 2018, pp. 153–179. doi:10.1016/b978-0-12-803581-8.09958-6.
URL https://doi.org/10.1016/b978-0-12-803581-8.09958-6

21

[2] Y. H. N. Kim, S. Ko, W.-S. Lay, J. Tian, P. Chang, S. U. Thielk, H.-J. Bang, J. Yang, Effects of shallow biangle, thin-ply laminates on structural performance of composite wings, AIAA Journal 55 (6) (2017) 2086–2092. doi:10.2514/1.j055465.
URL https://doi.org/10.2514/1.j055465

[3] A. Kopp, S. Stappert, D. Mattsson, K. Olofsson, E. Marklund, G. Kurth, E. Mooij, E. Roorda, The aurora space launcher concept, CEAS Space Journal 10 (2) (2017) 167–187. doi:10.1007/s12567-017-0184-2.
URL https://doi.org/10.1007/s12567-017-0184-2

[4] K. Kawabe, S. Tomoda, T. Matsuo, A pneumatic process for spreading reinforcing fiber tow, in: Proceedings of the 42nd International SAMPE Symposium and Exhibition, SAMPE, pp. 65–76.

[5] K. Kawabe, New spreading technology for carbon fiber tow and its application to composite materials, Sen'i Gakkaishi 64 (8) (2008) 262–267. doi:10.2115/fiber.64.p_262.
URL https://doi.org/10.2115/fiber.64.p_262

[6] K. Kawabe, H. Sasayama, S. Tomoda, New carbon fiber tow-spread technology and applications to advanced composite materials, SAMPE Journal 45 (2) (2008) 6–17.
URL https://researchmap.jp/?action=cv_download_main&upload_id=161885

[7] Simulia, Providence, RI, USA, ABAQUS/Standard User's Manual, Version 6.12 (2012).

[8] R. Krueger, Virtual crack closure technique: History, approach, and applications, Applied Mechanics Reviews 57 (2) (2004) 109. doi:10.1115/1.1595677.
URL https://doi.org/10.1115/1.1595677

[9] J. R. Rice, A path independent integral and the approximate analysis of strain concentration by notches and cracks, Journal of Applied Mechanics 35 (2) (1968) 379. `doi:10.1115/1.3601206`.
URL `https://doi.org/10.1115/1.3601206`

[10] C. Sandino, E. Correa, F. París, Numerical analysis of the influence of a nearby fibre on the interface crack growth in composites under transverse tensile load, Engineering Fracture Mechanics 168 (2016) 58–75. `doi:10.1016/j.engfracmech.2016.01.022`.
URL `https://doi.org/10.1016/j.engfracmech.2016.01.022`